Self-interstitial defects in hexagonal close packed metals revisited: Evidence for low-symmetry configurations in Ti, Zr, and Hf

G. Vérité,[1] C. Domain,[2,3,4] Chu-Chun Fu,[1] P. Gasca,[2,4] A. Legris,[2,4] and F. Willaime[1]

[1]*CEA, DEN, Service de Recherches de Métallurgie Physique, F-91191 Gif-sur-Yvette, France*

[2]*Unité Matériaux et Transformations, UMET UMR 8207, CNRS & Université Lille 1, F-59655 Villeneuve d'Ascq, France*

[3]*EDF R&D, Département MMC, Les Renardières, F-77250 Moret-sur-Loing, France*

[4]*Laboratoire commun EDF-CNRS Etude et Modélisation des Microstructures pour le Vieillissement des Matériaux (EM2VM), France*

(Received 28 January 2013; published 30 April 2013)

In addition to the eight conventional high-symmetry configurations for self-interstitials in the hexagonal close packed (hcp) structure, we show that four other configurations, obtained by breaking the symmetry of some of the original ones, may be low-energy local minima or saddle points. The first two, BC′ and C′, consist of the basal crowdion and the crowdion buckled perpendicular to their axes in the pyramidal plane, respectively. The two others, PS and P2S, are obtained by rotating the *c*-axis split dumbbell in the prismatic plane of first and second type, respectively. Using first-principles density functional theory calculations we show that BC′, C′, and PS are within 0.4 eV of the lowest-energy conventional structure, BO, in Ti, Zr, and Hf. BC′ could even be the lowest-energy configuration in hcp-Zr and its symmetry and possible reorientation mechanisms are compatible with internal friction measurements at variance with the conventional structures. The PS and C′ configurations exhibit a helicoidal easy glide motion of the dumbbell-crowdion type in the *c*-axis direction. These configurations therefore constitute an important element to take into account when predicting the microstructural evolution of zirconium-based materials under irradiation.

DOI: 10.1103/PhysRevB.87.134108 PACS number(s): 61.82.Bg, 61.72.jj, 31.15.A−

I. INTRODUCTION

The microstructural evolution of crystalline materials under irradiation is governed by the mobility of defects, of vacancy or interstitial type.[1,2] Self-interstitial atoms (SIA) in metals are quite challenging because their migration energy can vary from vanishing values to about half the value for vacancies depending on the stable structure, e.g., this is the case in body centered cubic (bcc) metals with the ⟨111⟩ crowdion and the ⟨110⟩ dumbbell, respectively.[3,4] In hcp-Zr, a fast diffusion of SIAs in the basal plane is often assumed to explain the observed radiation growth, a constant volume dimensional change.[1,5] Due to the technological importance in the nuclear industry of Zr alloys, which are used as cladding materials for pressurized water reactors, the behavior of hcp-Zr under irradiation has been particularly studied, both experimentally and by atomistic simulations.[5] However, no clear picture has emerged on the existing SIA structures and the dominant migration mechanism in this metal, and there are some contradictions between theory and experiments. According to Huang diffuse scattering experiments the SIA displacement field in hcp-Zr is nearly isotropic;[6] this excludes that only purely basal configurations are present in the material but no clear conclusion could be drawn on the SIA structures. Based on internal friction measurements in hcp-Zr, it was inferred that a SIA with two reorientation modes, with activation energies of 0.17 eV and 0.27 eV, respectively, is migrating in three dimensions with a migration energy of 0.3 eV.[7–9] This defect being sensitive to internal friction, its symmetry is orthorhombic, monoclinic, or triclinic. A monoclinic SIA was shown to be completely coherent with these measurements.[7,9] A similar behavior is observed in hcp-Ti.[7]

Atomistic simulations with empirical potentials have been widely used to study SIAs in hcp metals. In an early work, Johnson and Beeler proposed eight possible configurations:[10] the tetrahedral (T), octahedral (O), basal tetrahedral (BT), and basal octahedral (BO) interstitial sites; crowdions in and out of the basal plane (BC and C); and split dumbbells along the *c* axis (S) and in the basal plane (BS). The most stable structure depends on the potential. For instance in Zr, empirical potentials give either the C, BC, BS, O, or BO configurations.[11–16] More predictive calculations, based on the density functional theory (DFT), showed that in Zr four configurations have similar formation energies, within 0.2 eV: O, BO, BS, and S.[17–20] A similar result was obtained in Ti.[21] However, because of the strong and unusual size dependence observed between $N = 37$ and 97 atom cells, larger simulation cells must be used to determine the precise ordering of stability and energy differences.[22,23] Using conventional hexagonal cells, the most stable configuration at small sizes, $N = 37$, is O and it becomes BO above 97 atoms.[24,25] Above ∼150 atoms the energy of BS becomes comparable to that of O, or even lower depending on the calculation scheme; and up to the largest size investigated, 301 atoms, the ordering remains the same, i.e., BO, BS/O, and S, with all formation energies being within 0.3 eV.[24–26] The situation appears clearer from the DFT point of view, but this result is in contradiction with internal friction measurements. The O, BO, and S configurations are incompatible with experimental data because they are of hexagonal or trigonal symmetry (see Table I). The BS configuration is orthorhombic and can therefore be detected by internal friction, but its possible reorientation mechanisms are hardly compatible with experiments.

DFT has been successfully used recently to predict low-energy structures of defects in metals.[27–29] In this paper, based on DFT calculations in Ti, Zr, and Hf, we propose four low-symmetry and low-energy SIA configurations in the hcp structure. These metals belong to the same group, and they are therefore expected to display a similar behavior.

TABLE I. Symmetry and geometry of self-interstitial configurations in the hcp structure. The reduced coordinates are given for primitive vectors at 60° in the basal plane, and for lattice sites at (0,0,0) and (1/3,1/3,1/2). For dumbbell-type defects, i.e., BS, S, PS, PS′, and P2S, the atom at the origin is replaced by two atoms. Typical relaxed positions are given for S, BS, PS, PS′, BC′, P2S, and C′. The anisotropy ratio of the elastic dipole tensor, P_{33}/P_a, has been calculated using 289-atom cells with SIESTA in hcp-Zr. The last column gives the multiplicity (see text).

	Symmetry system	Point symmetry	Reduced coordinates	P_{33}/P_a	Multiplicity
BO	Hexagonal	$\bar{6}m2$	(2/3,–1/3,0)	0.56	1
O	Trigonal	$\bar{3}2/m$	(2/3,–1/3,1/4)	1.17	1
BS	Orthorhombic	$mm2$	(0.52,−0.22,0) (−0.31,0.07,0)	0.43	3
S	Orthorhombic	$\bar{6}m2$	(0,0,0.23) (0,0,−0.23)	1.93	1
C	Monoclinic	$2/m$	(1/6,1/6,1/4)	1.24	3
BC	Orthorhombic	$mm2$	(1/2,0,0)	–	3
T	Trigonal	$3m$	(0,0,3/8)	–	2
BT	Hexagonal	$\bar{6}m2$	(0,0,1/2)	–	1
BC′	Monoclinic	m	(0.62,−0.25,−0.08)	0.57	6
C′	Monoclinic	2	(0.31,0.02,1/4)	1.35	6
PS	Monoclinic	2	(0.24,0.04,0.21) (−0.19,−0.03,−0.21)	1.41	6
PS′	Monoclinic	2	(0.34,−0.06,0.15) (−0.28,−0.06,−0.15)	1.04	6
P2S	Monoclinic	m	(0.10,0.10,0.22) (−0.12,−0.12,−0.21)	1.42	6

II. METHODOLOGY

Most of the DFT results in Ti, Zr, and Hf reported here have been obtained with the VASP code in the projector augmented wave (PAW) framework with a kinetic-energy cutoff of 350 eV in Ti and 250 eV in Zr and Hf.[28–32] Tests performed in Zr showed that increasing the kinetic-energy cutoff to 400 eV changes the formation energies by ∼0.01 eV. Twelve electrons are included in the valence band for Ti and Zr, and 10 for Hf. A complementary DFT code, SIESTA,[33] has been used with the basis sets and pseudopotentials described in Ref. 34. All calculations are performed in the generalized gradient approximation (GGA) using the PW91 and PBE functionals for VASP and SIESTA, respectively.[35,36] For the Brillouin zone integration, we used the Methfessel-Paxton smearing scheme[37] with a smearing value of 0.2 eV for VASP and 0.3 eV for SIESTA.

Convergence tests were performed using supercells formed by $4\times4\times3$, $5\times5\times4$, $6\times6\times4$, $6\times6\times5$, and $7\times7\times5$ unit cells containing 97, 201, 289, 361, and 491 atoms, respectively, at constant rescaled volume, i.e., the volume of the cell containing a SIA is homogeneously rescaled with respect to the bulk equilibrium volume by a factor $(N+1)/N$ where N is the number of atoms in the bulk cell.[18] The k-point grids are $4\times4\times4$, $3\times3\times3$, $3\times3\times3$, $3\times3\times3$, and $3\times3\times3$, respectively, i.e., they correspond to a density not less than that of a $15\times15\times12$ grid for a 2-atom hcp unit cell. Constant pressure calculations with a high accuracy on stress tensor components, less than 0.2 kBar, have been performed with SIESTA with 97 atom cells to determine the formation volumes. The defect elastic dipole tensors, P_{ij}, were obtained from constant volume calculations as explained in Ref. 38 using SIESTA with 289 atom cells. The energy barrier calculations between two defect configurations have been performed using the drag method with SIESTA and 97 atom cells.

III. RESULTS

A. Geometry and symmetry of SIAs

The SIA configurations are obtained by breaking the symmetry of known SIA structures. For the first one, denoted BC′, the central atom of a BC defect is displaced perpendicular to the crowdion axis towards one of its two neighboring octahedral sites [Figs. 1(a) and 1(b)]. Displacing the atom along the c axis also yields a BC′ configuration after relaxation. There are six BC′ sites around each O or BO site. In a similar way, the second configuration, denoted C′, is obtained by shifting the central atom of a C crowdion towards an O site [Figs. 1(c) and 1(d)]. BC′ and C′ can be seen as buckled crowdions, spread in the pyramidal plane. The other configurations are obtained by rotating the S split dumbbell in the prismatic plane of type 1, P1, i.e., towards the BS configuration, and type 2, P2, respectively [Figs. 1(e)–1(h)]. The typical energy landscape with respect to these rotations is illustrated in Fig. 2 by SIESTA calculations in Zr. For the P1 rotation, between the S and BS local minima, two other minima, denoted PS and PS′, are found around 30° and 50° with respect to the c axis, respectively. For simplicity, only the lower of these two minima will be considered in the following. The local minimum for the P2 rotation, denoted P2S, is around 30°.

A common point to the SIA configurations, BC′, C′, PS, and P2S, is that they have a larger multiplicity. For each of them, there are six possible sites and/or orientations per lattice site, instead of only one for O, BO, and S and three for BS (see Table I). This larger multiplicity will therefore increase their relative concentrations under local equilibrium conditions: At room temperature a configuration with a multiplicity of 6 has a concentration equal to that of a configuration 0.04 eV lower in energy with a multiplicity of 1. The symmetries and geometry characteristics of all configurations are summarized in Table I.

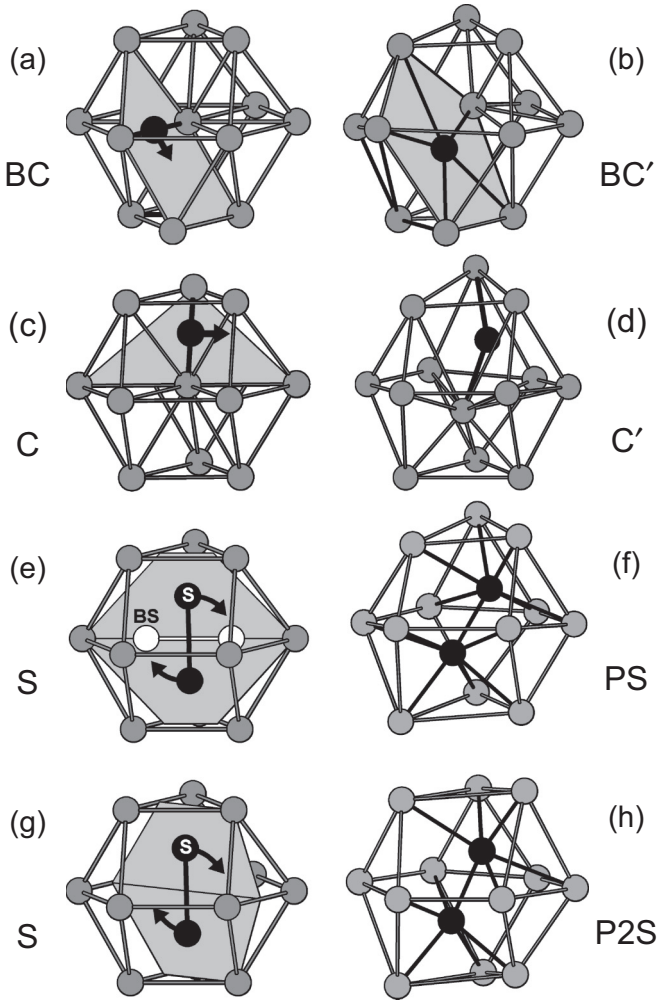

FIG. 1. Schematic of the proposed low-symmetry configurations for self-interstitials in the hcp structure. (a), (c), (e), and (g) Original unrelaxed BC, C, and S configurations; the arrows indicate the direction of the displacement of the central atom that breaks the defect symmetry in (a) and (c) and the rotation direction in (e) and (g). (b), (d), (f), and (h) Structures after relaxation of the BC′, C′, PS, and P2S configurations.

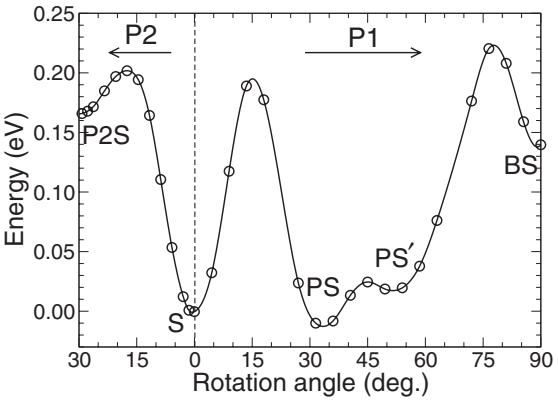

FIG. 2. Energy landscape obtained by rotating a S split dumbbell in the prismatic plane of type 1 (right) and type 2 (left), see Figs. 1(e) and 1(g). Calculations have been performed in hcp-Zr with the SIESTA code using a 97-atom cell and relaxing the system with a constraint on the angle of the dumbbell with respect to the c axis.

B. DFT energetics of SIAs

The formation energies of all configurations have been calculated within DFT for Ti, Zr, and Hf. BC decays to BO in Zr and Hf and to BS in Ti, T decays to S, and BT has either a high energy or decays to BO. The results obtained for all the other configurations are summarized in Table II. For the conventional configurations the formation energy differences agree very well with previous calculations in Zr (Refs. 18,19,24,25) and Ti.[21] Cell-size convergence in Zr shows that formation energies evolve only weakly beyond 289 atoms; the discrepancies with larger cell sizes are expected to be comparable to uncertainties due to exchange-correlation functional or pseudopotential/PAW data sets. For the main purpose of the present paper, which is to show that the configurations described in Sec. III A have formation energies comparable to that of conventional structures, the 289-atom cell proves to be sufficient.

The results obtained for the SIA formation energies in Ti, Zr, and Hf with VASP are illustrated in Fig. 3. As already noticed in bcc metals[39] the SIA formation energy increases significantly from 3d to 5d metals, but the relative stabilities of the various structures display the same trends in Ti, Zr, and Hf. The remarkable result, that we shall discuss in more detail below, is that BC′, C′, and PS have formation energies comparable to that of BO, BS, O, and S. The energy differences with the BO structure—except for O—are smaller in Zr. In other words the BO and O formation energies relative to the averages over all configurations are higher in Zr than in Ti and Hf. Although this does not follow any obvious chemical trend, one may notice that this is also the case for other structural properties such as the c/a ratio. All these characteristics are perfectly reproduced with SIESTA, in spite of the approximation made in the single-projector pseudopotential and reduced basis set.

The formation energy of BC′ is particularly low in Zr: It is lower than that of O and BS, and it is almost equal to that of BO, within 0.02 eV, according to VASP. In Ti and Hf, BC′ is also a low-energy local minimum with VASP whereas it decays to BO with SIESTA. Central to the link with internal friction experiments in Zr is the monoclinic symmetry of the BC′ configuration. Moreover this defect can display at least two reorientation modes: The central atom of the defect can shift to an equivalent site either across the basal plane or within the basal plane. These mechanisms are therefore very good candidates to account for the reorientation peaks observed in internal friction experiments.

The tendency of C to buckle into C′ is such that C is not a local minimum but a saddle point between two C′ configurations in Ti, Zr, and Hf according to the present DFT calculations. This is not an electronic structure effect since we found that it is also the case with an empirical potential for Zr,[40] where C′ is even the lowest-energy structure.[22] The C′ and PS configurations are closely connected to each other: The two nearest-neighbor pairs of atoms of a C′ defect can be associated with two PS defects, with appropriate orientations centered on either of the two lattice sites of the C′ defect, respectively (Fig. 4). Very small atomic displacements are required to go from PS to C′ and the energy difference between these two defects is very small (see Fig. 3 and Table II). Moreover, according to SIESTA, the energy landscape connecting them is completely flat within 0.01 eV in Zr. The PS-C′-PS-C′

TABLE II. DFT formation energies of SIAs in Ti, Zr, and Hf in the hcp structure (in eV). The formation energy is given for BO, and the energy difference with respect to BO is given for the other configurations. The BC′ configuration decays to BO in Ti and Hf in SIESTA calculations. The code, VASP, SIESTA, or QUANTUMESPRESSO (QE), and the number of atoms are given in the second and third columns.

		N	E_{BO}	E_O-E_{BO}	E_{BS}-E_{BO}	E_S-E_{BO}	E_C-E_{BO}	$E_{BC'}$-E_{BO}	$E_{C'}$-E_{BO}	E_{PS}-E_{BO}	E_{P2S}-E_{BO}
Ti	SIESTA	289	2.42	0.14	0.26	0.28	0.50	BO	0.34	0.36	0.51
	VASP	289	2.29	0.11	0.17	0.36	0.53	0.16	0.36	0.38	0.60
	VASP	361	2.29	0.11	0.17	0.32	0.54	0.16	0.32	0.34	0.55
	VASP	491	2.27	0.11	0.18	0.35	–	0.17	0.36	0.37	0.59
Zr	SIESTA	97	3.21	0.04	0.22	0.07	0.26	0.09	0.09	0.08	0.26
	SIESTA	289	3.03	0.13	0.23	0.17	0.40	0.09	0.24	0.25	0.40
	VASP	97	2.93	0.00	0.12	0.21	0.38	0.07	0.15	0.15	0.40
	VASP	201	2.78	0.09	0.11	0.23	0.45	0.03	0.22	0.23	0.44
	VASP	289	2.70	0.11	0.09	0.22	0.44	0.02	0.23	0.24	0.44
	VASP[a]	289	2.78	0.14	0.09	0.30	–	–	–	–	–
	QE[b]	301	2.75	0.16	0.14	0.22	–	–	–	–	–
	VASP	361	2.73	0.11	0.09	0.20	0.42	0.02	0.22	0.22	0.42
	VASP	491	2.70	0.14	0.09	0.24	–	0.03	0.27	–	–
Hf	SIESTA	289	4.04	0.43	0.38	0.37	0.60	BO	0.39	0.38	0.61
	VASP	289	3.90	0.36	0.22	0.56	0.67	0.16	0.37	0.34	0.66
	VASP	361	3.87	0.34	0.21	0.52	0.65	0.12	0.31	0.29	0.60
	VASP	491	3.86	0.36	0.22	0.54	–	0.17	0.38	0.35	0.66

[a]Reference 24.
[b]Reference 25.

sequence therefore constitutes an easy glide mechanism along the c axis, where the center of the defect exhibits a helicoidal motion (Fig. 4). This mechanism is analogous to the fast one-dimensional (1D) glide involving ⟨111⟩ dumbbells and crowdions in the bcc structure. However, according to DFT calculations in Zr, the energy difference with the lowest-energy structure, BO or BC′, is approximately 0.25 eV. The most likely scenario is therefore that, in competition with other migration mechanisms, the defect goes first from BO or BC′ to PS or C′ by thermal activation, and then performs a fast 1D-type glide along the c axis over a few interatomic distances before returning to BO or BC′.

Finally, the P2S configuration is not a local minimum within DFT, but a saddle point between two PS configurations. The instability of the P2S structure within DFT can be related to the sharp peak at the Fermi level in the local density of states of the SIAs; it is therefore not surprising that this configuration can, on the contrary, be a low-energy local minimum with empirical potentials.[22]

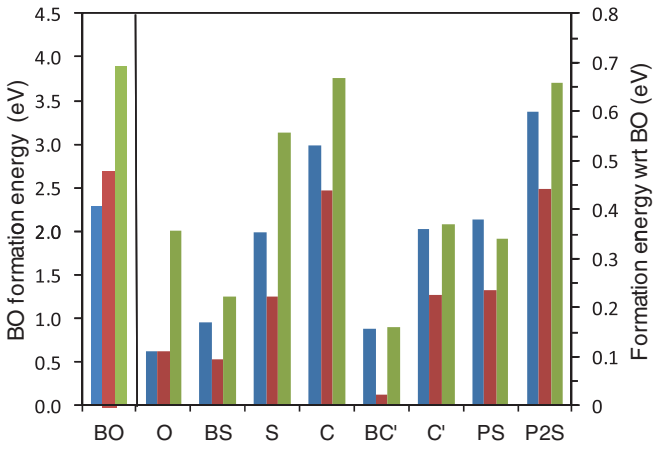

FIG. 3. (Color online) DFT formation energies of SIAs in hcp Ti (blue), Zr (red), and Hf (green). (Left) Formation energies of the reference BO configuration. (Right) formation energies relative to the BO configuration of the O, BS, S, C, BC′, C′, PS, and P2S configurations. All energies correspond to the VASP-PAW calculations with 289-atom cells. Similar results are obtained with SIESTA (see Table II).

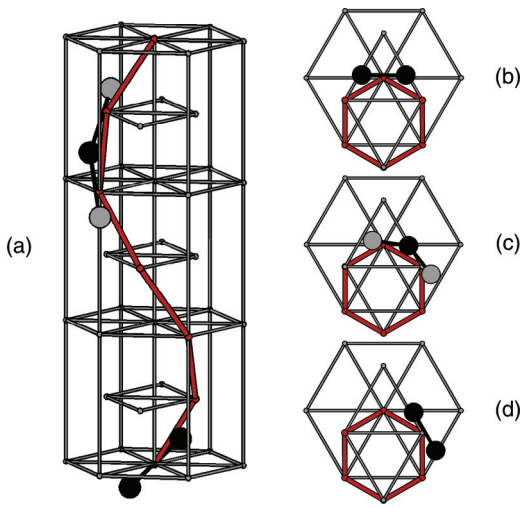

FIG. 4. (Color online) Easy glide mechanism in the c-axis direction by a helicoidal PS-C′ motion. (a) Schematic of the trajectory in red with a PS dumbbell at the bottom and a C′ buckled crowdion in the upper part. (b), (c), and (d) Top views of a PS-C′-PS migration sequence.

TABLE III. DFT formation volumes of SIAs in Ti, Zr, and Hf in the hcp structure, calculated with SIESTA and 97-atom cells. The volumes are expressed in units of atomic volume, Ω_0. The average volume is given in the last column.

	BO	O	BS	S	C	BC′	C′	PS	P2S	Average
Ti	0.00	0.03	0.01	0.01	0.04	0.02	0.06	0.05	0.07	0.03
Zr	0.12	0.17	0.18	0.04	0.11	0.14	0.12	0.12	0.08	0.12
Hf	0.17	0.31	0.25	0.17	0.27	0.24	0.27	0.28	0.28	0.25

These configurations are expected to play an important role in the migration mechanisms, since they can be intermediate configurations along the path between conventional configurations; this is how they were evidenced first in the present study. Unlike what could be expected from the fact that the three lowest-energy structures, BO, BC′, and BS, are essentially basal configurations, no fast basal migration of the SIA was evidenced from preliminary calculations.[22,23]

C. DFT formation volumes and elastic dipole tensors of SIAs

The formation volume, Ω_f, is calculated as

$$\Omega_f = \Omega(N+1,1) - \frac{N+1}{N}\Omega(N,0),$$

where $\Omega(N+1,1)$ and $\Omega(N,0)$ are the equilibrium volumes of a system containing $N+1$ atoms and one SIA and N bulk atoms, respectively. The results obtained in Ti, Zr, and Hf are summarized in Table III. The formation volumes are found to increase from Ti to Hf: The average values are 0.03 Ω_0 in Ti, 0.12 Ω_0 in Zr, and 0.25 Ω_0 in Hf, where Ω_0 is the equilibrium atomic volume. The formation volumes are small for all configurations in the three metals, and comparable for all configurations for a given metal. The small value of the formation volume is consistent with experiments in hcp-Zr.[6]

The elastic dipole tensor gives useful information on the anisotropy of the SIA displacement fields. The ratio between the c and basal plane components of the elastic dipole tensor is given by P_{33}/P_a, where $P_a = [2(P_{11}^2 + P_{22}^2 + 2P_{12}^2) + (P_{11} + P_{22})^2]^{1/2}/8$.[6] The DFT results obtained in hcp-Zr for P_{33}/P_a are reported in Table I. The values for the two lowest-energy structures, BO and BC′, as well as for BS, which are basal or mostly basal, are smaller than 0.6, whereas they are larger than 1.2 for O, S, and PS/C′. These results can be compared to data obtained from Huang diffuse scattering experiments, which led to a value of $P_{33}/P_a = 1.1 \pm 0.2$.[6] It can therefore be inferred from this comparison that at least one configuration from the second set coexists with the lowest-energy BO and BC′ structures in hcp-Zr under irradiation.

IV. CONCLUSIONS

Based on DFT calculations in Ti, Zr, and Hf, low-energy and low-symmetry structures for self-interstitials are proposed in hcp metals. The configuration obtained by buckling BC towards an O site, denoted BC′, is shown to have a particularly low energy, i.e., within 0.02 eV of the lowest-energy structure BO in Zr according to VASP, and within 0.15 eV in Ti and Hf. This monoclinic configuration is a good candidate to explain the internal friction measurements, unlike the BO configuration. Two configurations, denoted C′ and PS, are within 0.25 to 0.3 eV of BO and display a helicoidal easy glide motion in the c-axis direction. They are obtained by buckling C towards an O site and by rotating S towards BS, respectively. The anisotropy ratio of the elastic dipole tensor of all possible SIA configurations ranges from 0.4 for BS to 2 for S. From the experimental value proposed for this ratio from Huang scattering experiments, the present results suggest that in hcp-Zr under irradiation several configurations should coexist, including BO, BC′, and BS, and at least one configuration from the set made by O, S, and C′-PS. This large number of coexisting configurations together with the rather slow character of the convergence of the formation energies with supercell size make the study of SIA migration in hcp-Zr particularly challenging.

ACKNOWLEDGMENTS

G.V. and F.W. acknowledge D. Gratias (LEM, CNRS-ONERA, Châtillon, France) for his help with the symmetry analysis of the defect configurations. P.C. and A.L. acknowledge EDF R&D (project "Matériaux de l'assemblage") for financial support. Some of the calculations were performed at the CRI-Lille 1 University supported by the Fonds Européens de Développement Régional. E. Clouet and C. Varvenne (CEA, France) are acknowledged for fruitful discussions and E. Hayward for critical reading of the manuscript.

[1] G. S. Was, *Fundamentals of Radiation Materials Science* (Springer-Verlag, Berlin, 2007).
[2] C. C. Fu, J. Dalla Torre, F. Willaime, J.-L. Bocquet, and A. Barbu, Nat. Mater. **4**, 68 (2005).
[3] S. P. Fitzgerald and D. Nguyen-Manh, Phys. Rev. Lett. **101**, 115504 (2008).
[4] C. C. Fu, F. Willaime, and P. Ordejon, Phys. Rev. Lett. **92**, 175503 (2004).
[5] F. Onimus and J. L. Béchade, in *Comprehensive Nuclear Materials*, edited by R. Konings (Elsevier, Oxford, 2012), Vol. 4, pp. 1–31.
[6] P. Ehrhart and B. Schönfeld, in *Point Defects and Defect Interactions in Metals*, edited by I. Tokamura, M. Doyama, and M. Kiritani (University of Tokyo Press, Tokyo, 1982), pp. 47–52.
[7] R. Pichon, E. Bisogni, and P. Moser, Radiat. Eff. **20**, 159 (1973).
[8] R. Pichon, Ph.D. thesis, Grenoble University, 1973.
[9] P. Moser and R. Pichon, J. Phys. F **3**, 363 (1973).

[10]R. A. Johnson and J. R. Beeler, in *Interatomic Potentials and Crystalline Defects*, edited by J. K. Lee (AIME, New York, 1981), pp. 165–177.
[11]D. Bacon, J. Nucl. Mater. **159**, 176 (1988).
[12]F. Willaime and C. Massobrio, Phys. Rev. B **43**, 11653 (1991).
[13]M. Igarashi, M. Khantha, and V. Vitek, Philos. Mag. B **63**, 603 (1991).
[14]G. J. Ackland, S. J. Wooding, and D. J. Bacon, Philos. Mag. A **71**, 553 (1995).
[15]Y. M. Kim, B. J. Lee, and M. I. Baskes, Phys. Rev. B **74**, 014101 (2006).
[16]C. H. Woo and X. Liu, Philos. Mag. **87**, 2355 (2007).
[17]C. Domain, Ph.D. thesis, Lille 1 University, 2002.
[18]F. Willaime, J. Nucl. Mater. **323**, 205 (2003).
[19]C. Domain and A. Legris, Philos. Mag. **85**, 569 (2005).
[20]Note that the configuration reported as BC in Ref. 19 corresponds in fact to a BS configuration.
[21]A. T. Raji, S. Scandolo, R. Mazzarello, S. Nsengiyumva, M. Härting, and D. T. Britton, Philos. Mag. **89**, 1629 (2009).
[22]G. Vérité, Ph.D. thesis, Université Pierre et Marie Curie, Paris, 2007.
[23]P. Gasca, Ph.D. thesis, Lille 1 University, 2010.
[24]Q. Peng, W. Li, H. Huang, and S. De, J. Nucl. Mater. **429**, 233 (2012).
[25]G. D. Samolyuk, S. I. Golubov, Y. N. Osetsky, and R. E. Stoller, Philos. Mag. Lett. **93**, 93 (2013).
[26]C. Varvenne and E. Clouet (private communication, 2012).
[27]D. A. Terentyev, T. P. C. Klaver, P. Olsson, M.-C. Marinica, F. Willaime, C. Domain, and L. Malerba, Phys. Rev. Lett. **100**, 145503 (2008).
[28]M. C. Marinica, F. Willaime, and J. P. Crocombette, Phys. Rev. Lett. **108**, 025501 (2012).
[29]H. Wang, D. Rodney, D. Xu, R. Yang, and P. Veyssière, Phys. Rev. B **84**, 220103(R) (2011).
[30]G. Kresse and J. Furthmuller, Phys. Rev. B **54**, 11169 (1996).
[31]G. Kresse and J. Furthmuller, Comput. Mater. Sci. **6**, 15 (1996).
[32]G. Kresse and D. Joubert, Phys. Rev. B **59**, 1758 (1999).
[33]J. M. Soler, E. Artacho, J. D. Gale, A. Garcia, J. Junquera, P. Ordejon, and D. Sanchez-Portal, J. Phys.: Condens. Matter **14**, 2745 (2002).
[34]G. Vérité, F. Willaime, and C. C. Fu, Solid State Phenomena **129**, 75 (2007).
[35]J. P. Perdew, J. A. Chevary, S. H. Vosko, K. A. Jackson, M. R. Pederson, D. J. Singh, and C. Fiolhais, Phys. Rev. B **46**, 6671 (1992).
[36]J. P. Perdew, K. Burke, and M. Ernzerhof, Phys. Rev. Lett. **77**, 3865 (1996).
[37]M. Methfessel and A. T. Paxton, Phys. Rev. B **40**, 3616 (1989).
[38]E. Clouet, S. Garruchet, H. Nguyen, M. Perez, and C. S. Becquart, Acta Mater. **56**, 3450 (2008).
[39]D. Nguyen-Manh, A. P. Horsfield, and S. L. Dudarev, Phys. Rev. B **73**, 020101(R) (2006).
[40]M. I. Mendelev and G. J. Ackland, Philos. Mag. Lett. **87**, 349 (2007).